UKR Journal of Multidisciplinary Studies (UKRJMS)
Homepage: https://ukrpublisher.com/ukrjms/
Email: submit.ukrpublisher@gmail.com
Volume 2, Issue 6, 2026
ISSN: 3049-432X (Online)
OPEN ACCESS

Predictions with CFD simulations at full scale of Speed and delivered power in waves

Dr. Gunamani B. Deheri[1]; Dr. Dhinesha Ruwanthi Perera[2]; Dr. Pragna A. Vadher[3]; Dr. Narendra Kumar[4]; Dr. Priti Vasantbhai Tandel[5]; Rakesh Manilal H. Patel[6]

[1] Retired Associate Professor of Mathematics, Department of Mathematics, Sardar Patel University, Vallabh Vidyanagar, Gujarat, India. Email ID: gm.deheri@rediffmail.com

[2] Senior Lecturer, Department of Management and Finance, General Sir John Kotelawala Defence University, Sri Lanka. Email ID: dhinesha_drp@kdu.ac.lk

[3]Principal, Government Science College, Idar, Gujarat, India. Email ID: pragnavadher@gmail.com

[4]IILM University, Greater Noida, NCR, India.

[5]Assistant Professor of Mathematics, Department of Mathematics, Veer Narmad South Gujarat University, Surat, Gujarat, India.

[6] Government Science College, Sector-15, Gandhinagar, Gujarat, India.

***Corresponding Author**: Dr. Gunamani B. Deheri, Email ID: gm.deheri@rediffmail.com

DOI: *https://doi.org/10.5281/zenodo.20907503*

Article History

Original Research Article

Received: 01-04-2026

Accepted: 04-05-2026

Published: 26-06-2026

Citation: Dr. Gunamani B. Deheri, Dr. Dhinesha Ruwanthi Perera, Dr. Pragna A. Vadher, Dr. Narendra Kumar, Dr. Priti Vasantbhai Tandel & Rakesh Manilal H. Patel. (2026). Predictions with CFD Simulations at Full Scale of Speed and Delivered Power in Waves. UKR Journal of Multidisciplinary Studies (UKRJMS), 2(6), 324-339.

Abstract

This study proposes a general numerical tool for assessing the propulsion performance of ships in wind–wave conditions, focusing on delivered power demands and speed loss. This method uses an unsteady potential-flow panel formulation to determine wave-induced resistance and combined with a steady-state potential-flow/Reynolds-Averaged Navier–Stokes (RANS) methodology including body-force representation of the propeller for simulating self-propulsion characteristics to estimate the resistance in calm water. Comparisons between numerical results and experimental measurements for added resistance, calm-water resistance and delivered power served to evaluate the reliability of the procedure, showing a high degree of agreement. To show further applicability of the developed method, here it is applied to estimate a weather correction factor f_w which is needed for the Energy Efficiency Design Index (EEDI) [1] The f_w predictions resulting there from show very smooth agreement with values calculated from full scale operational records of similar vessel types, suggesting that not only is the method suitable for design stage assessments but also for exploratory performance evaluations in realistic environmental conditions.

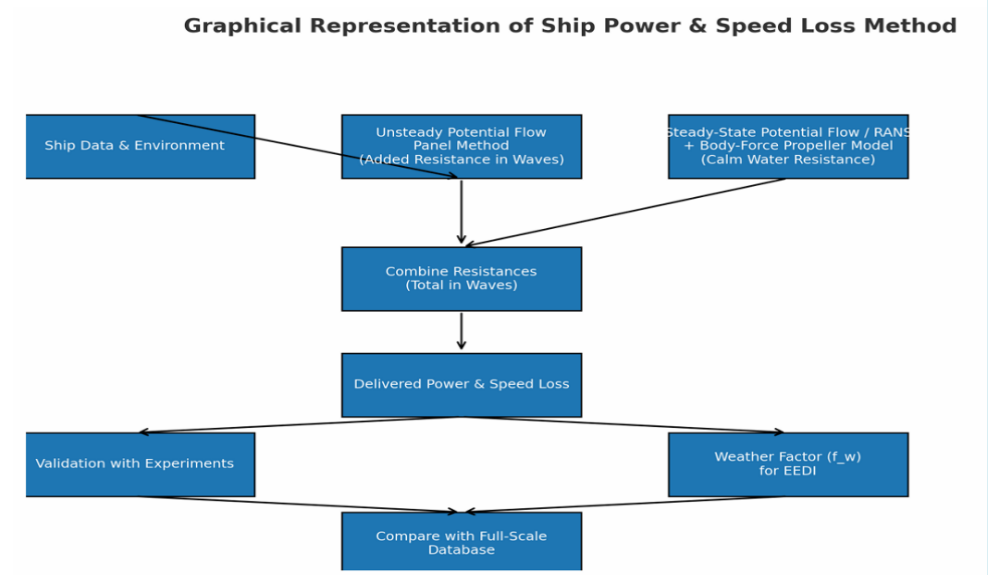

Keywords: *Sea keeping (SK), EEDI (Energy Efficiency Design Index), Weather factor, Delivered power (WFDP), Speed loss (SL), Full-scale measurements (FSM), Self-propulsion tests (SPT).*

Subject classification:

Engineering → Mechanical Engineering → Marine / Naval Architecture Computational Science → Computational Fluid Dynamics (CFD) Applied Physics → Fluid Mechanics → Hydrodynamics Transportation Engineering → Ship Performance and Propulsion, Naval Architecture, Marine & Ocean Engineering, Computational Fluid Dynamics (CFD), Ship Resistance and Propulsion, Sea keeping and Performance in Waves.

Nomenclature:

ω *Specific turbulence dissipation rate*
CF *Frictional resistance coefficient*
CP *Pressure resistance coefficient*
CT *Total resistance coefficient*
CAW *Added resistance in waves coefficient*
fw *Weather factor*
k *Turbulent kinetic energy*
kS *Equivalent sand grain roughness height*
ng *Number of grid cells*
PD *Delivered power*
UG *Grid uncertainty*

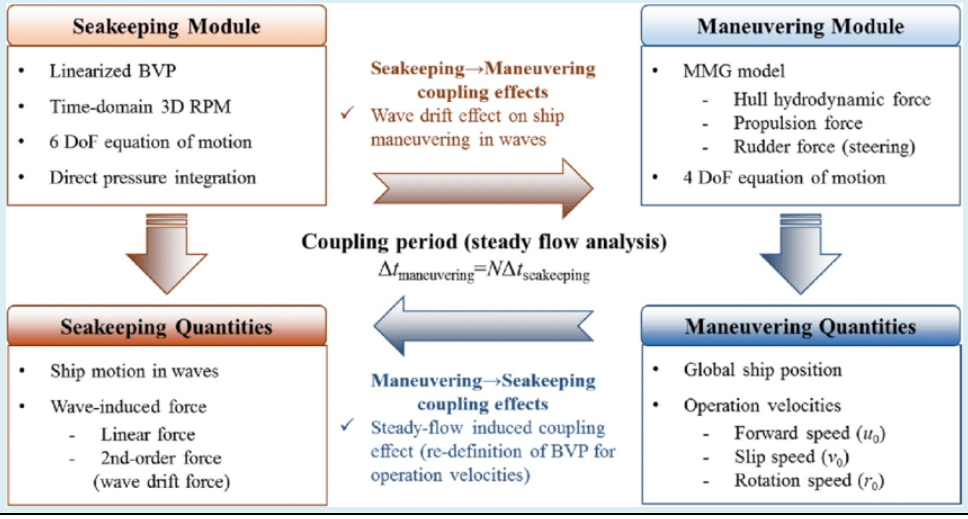

Introduction

Over the past several decades, Computational Fluid Dynamics (CFD) has matured into a modern and well-established methodology for estimating ship resistance and propulsors characteristics in model scale under calm-water conditions. It has been documented in detail through successive International Workshops on Numerical Ship Hydrodynamics (Larsson et al., 2014; Hino et al., 2021). Model-scale predictions are capable of providing guidance, however the determination of full-scale performance typically requires procedures that account for scale effects. Recently, simulation has gained more attention to conducting at full scale, with the most extensive validation initiative currently pursued in Joint Research Project on Development of Industry-recognised Benchmarks for Ship Energy Efficiency Solutions (JoRes, 2023). Prior studies have also shown the practical feasibility of full-scale numerical modelling (Orych et al., 2021). On the other hand, from a design perspective an accurate prediction of vessel behaviour in actual operational conditions is more important than from a physics standpoint (due to wind and wave actions). Previous evaluations of seakeeping performance have primarily been conducted through controlled experimental studies performed in towing tanks and model basins; however, with advancements in numerical techniques, these simulations are now becoming a more common approach. These computational

approaches facilitate applications like the estimation of ITTC (2021b) weather factor prescribed to be employed in the EEDI calculation (IMO, 2018), as well as for conditional calm-water reference speed determination within Energy Efficiency Existing Ship Index – EEXI framework (IMO, 2022). Essentially, numerical methods are categorized based on governing assumptions and computational requirements in Figure 1.

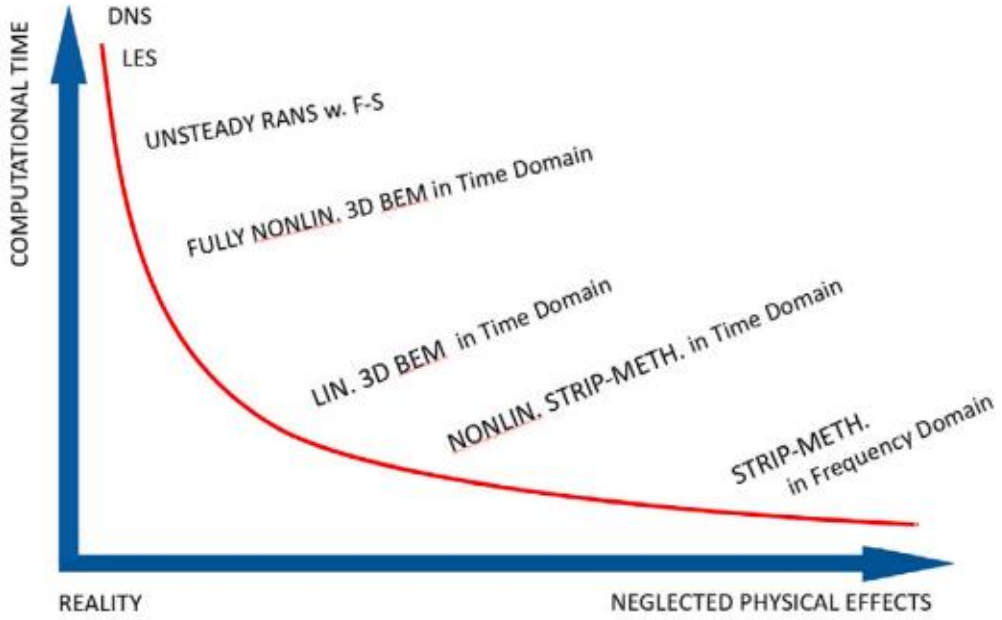

Figure 1. Computational methods for seakeeping

Among the different available methodologies for seakeeping type studies, frequency-domain strip theory is the least computationally expensive and can quickly yield results using modern computational power. The nonlinear strip method, its time-domain counterpart, improves this capabilityin most scenarios. In more advanced and specific methods, it is worth noting the three-dimensional Boundary Element Methods (BEM), that can be applied in linear and fully non-linear forms. In addition to these methods, unsteady Reynolds-Averaged Navier–Stokes (RANS) simulations offer a more precise description of fluid dynamics and ship motions at greatly increased computational effort. The Large Eddy Simulation (LES) and Direct Numerical Simulation (DNS) methods make up the extreme upper end of the computational pyramid, but both remain impractical for everyday industrial applications due to their substantive resource requirements. Currently, nonlinear BEM and RANS methods provide the best trade-off between simulation accuracy and computational cost. Turbulence interacting with the hull surface is often maelstrom in high-speed vessels and thus RANS based analyses are more widely accepted into industry; however, simulation convergence necessitates an extensive computation time to complete enough simulations. As a result, hybrid modelling approaches have arisen as a promising direction. For instance, Kim et al. Massé et al. (2017) used a combination of linear two- and three-dimensional potential-flow techniques along with unsteady RANS simulations to predict wave-induced added resistance, employing simplified procedures for estimating calm-water resistance and speed reduction. In a similar approach by Saettone (2020), the researcher combined an unsteady potential-flow solver based on six-degrees-of-freedom motion with a two-model RANS framework and a boundary-element propeller analysis tool to show that hybrid methodologies can yield accurate estimates of average propulsive power in moderate sea states. Some studies have integrated different simulation elements of a similar computational environment (e.g., Zhang & Kim, 2018) but simulating such complex interactions for kinematic seakeeping evaluations would currently be impractical. Therefore, aerodynamic resistance due to wind is usually considered a force acting outside the body (an external resistance term) in self-propulsion studies and can be determined from wind-tunnel data, computational fluid dynamics or empirical models (ITTC, 2021b). Based on these advances, the current research introduces a coupling of BEM and RANS for full-scale ship propeller performance assessment in real seas, focusing on speed loss predictions. The method employs a recently developed 2D fully nonlinear unsteady potential-flow solver for free-surface flows in the region around floating bodies undergoing six-degree-of-freedom motion (Coslovich et al., 2021). The wave-induced added resistance from this solver is then merged with a potential-flow evaluation of calm-water wave resistance and finally, with a clear water condition double-model steady-state RANS solution for full scale self-propulsion similar to the RANSE-RM-

coupled hydrodynamic assessment algorithm. The proposed framework is more than one order of magnitude cheaper in terms of computational cost while achieving similar levels of predictive accuracy as compared with conventional unsteady RANS simulations. This trade-off of balance between efficiency and reliability makes the method very well appropriate for practical plan approval studies and regulatory assessments, such as in Energy Efficiency Design Index (EEDI) compliance applications. However, the study is limited to normal operating conditions and does not cover vessel behaviour under severe survival or emergency conditions.

CFD simulations at full scale of speed and delivered power in waves — mathematical approach

1. Scope and assumptions

1. Newtonian incompressible fluid (ρ, μ constant).
2. Free surface with air above; two-phase flow modeled with a surface-capturing method (VOF or level-set).
3. Body (ship or wave energy device) is rigid; motion may be prescribed (fixed speed) or solved (6-DOF).
4. Waves can be regular or irregular; linear wave theory used to prescribe far-field / incident waves for initialization.
5. Propulsion: propeller and machinery modeled either via actuator disk (for large domains) or explicit geometry (if resolved). Propulsive efficiency η prop applies to convert required shaft power to delivered shaft power.
6. Viscous and potential effects both retained via URANS (or DES / LES if needed).

2. Governing equations

Two-phase incompressible Navier–Stokes with a volume fraction field α(x, t) (α = 1 water, α = 0 air).

Continuity:

$\nabla \cdot u = 0$

Momentum (one-field variable density/viscosity):

$$\frac{\partial(\rho u)}{\partial t} + \nabla \bullet (\rho u \otimes u) = -\nabla p + \nabla \bullet \tau + \rho g + f_{SGS}$$

where $\tau = \mu (\nabla u + (\nabla u)^T)$ Use appropriate turbulence model (URANS k – ω SST recommended for separated flows).

VOF advection for α:

$$\frac{\partial \alpha}{\partial t} + u \bullet \nabla \alpha = 0$$

Fluid properties:

$\rho(x, t) = \alpha\rho_w + (1 - \alpha)\rho_a$, $\mu(x, t) = \alpha\mu_w + (1 - \alpha)\mu_a$.

3. Free-surface and wave boundary conditions

For regular incident waves (height H, period T, propagation in +x):

Linear (Airy) wave theory in deep water:

- Free-surface elevation: $\eta(x, t) = 0.5H\cos(kx - \omega t)$
- Dispersion: $\omega^2 = gk\tanh(kh)$ (deep water: $\tanh(kh) \to 1$)
- Horizontal / vertical velocities from potential function.

At inlet impose time-varying velocity and α consistent with wave theory (or use internal wave generator). At outlet use wave absorption (sponge layer, relaxation zone) to avoid reflections.

4. Non-dimensionalization and key numbers

Let characteristic length L (ship length or device characteristic), speed U (vessel speed in calm water), gravity g.

Important non-dimensional numbers:

- Froude number: $F_r = \frac{U}{\sqrt{gL}}$ — governs wave making.
- Reynolds number: $R_e = \frac{\rho UL}{\mu}$ — viscous effects.
- Keulegan–Carpenter (for oscillatory flows): $KC = \frac{U_m T}{D}$ (if oscillatory velocity U_m and diameter D).
- Wave steepness: 0.5kH (should be small for linear theory).

Scaling remark: full-scale CFD is expensive but necessary when Reynolds or nonlinear wave affects are critical; otherwise use model tests + Froude scaling carefully and account for Reynolds mismatch (append model for friction correction).

5. Power definitions

5.1 Incident wave power (per unit crest length)

Energy density of linear waves: $E = \frac{1}{8}\rho g H^2$

Group velocity c_g (deep water): $c_g = \frac{gT}{4\pi} = 0.5c, here\ c = \frac{0.5gT}{\pi}$

Therefore incident wave power per unit crest:

$$P_{inc} = Ec_g = \frac{\rho g^2 H^2 T}{32\pi}$$

(Useful for capture width / wave energy converter benchmarking.)

5.2 Hydrodynamic forces and instantaneous power on a body

Hydrodynamic force on body surface S_b:

$$F(t) = \int_{S_b} [-pn + \tau \bullet n] dS$$

If body has surge (forward) velocity $U_b(t)$ relative to fixed coordinates, instantaneous power transferred from fluid to body (mechanical power input to propulsion or PTO) is:

$$P_{hyd}(t) = F(t) \bullet U_b(t) + \int_{S_b} \tau \bullet n \bullet U_b(t) dS$$

More generally, instantaneous power delivered to the body (positive when fluid does work on body) is:

$$P_{hyd}(t) = \int_{S_b} \{-pn + \tau \bullet n\} \bullet U_b(t) dS$$

where $u_b$is local surface velocity of the body (for rigid body $u_b = U_{trans} + \omega \times r$).

If body is constrained to constant forward speed U (e.g., steady propulsion), the mean delivered shaft power required to maintain that speed against hydrodynamic resistance is:

$$P^*_{req} = \frac{R^*_{tot} U}{\eta_{prop}}$$

where R_{tot} is time-averaged total resistance (calm + wave-induced + added resistance due to motions) and η_{prop} is propulsive efficiency.

5.3 Practical computation of mean delivered power in waves (CFD postprocessing)

1. Compute instantaneous surge force
$$F_x(t) = \int_{S_b} \{-pn_x + (\tau \bullet n)_x\} dS$$
2. If vessel forward velocity is U(body velocity relative to water), instantaneous power to overcome hydrodynamic load:

   $P(t) = F_x(t)\, U$.
3. Mean delivered power over N wave periods:
$$P^* = \frac{1}{T_{avg}} \int_{t_0}^{t_0 + T_{avg}} P(t) dt$$

   (choose T_{avg} multiple of wave period).
4. Convert to shaft power:
$$P^*_{shaft} = \frac{P^*}{\eta_{prop}}$$

If propeller modeled, compute torque / power directly from resolved propeller or actuator disk model.

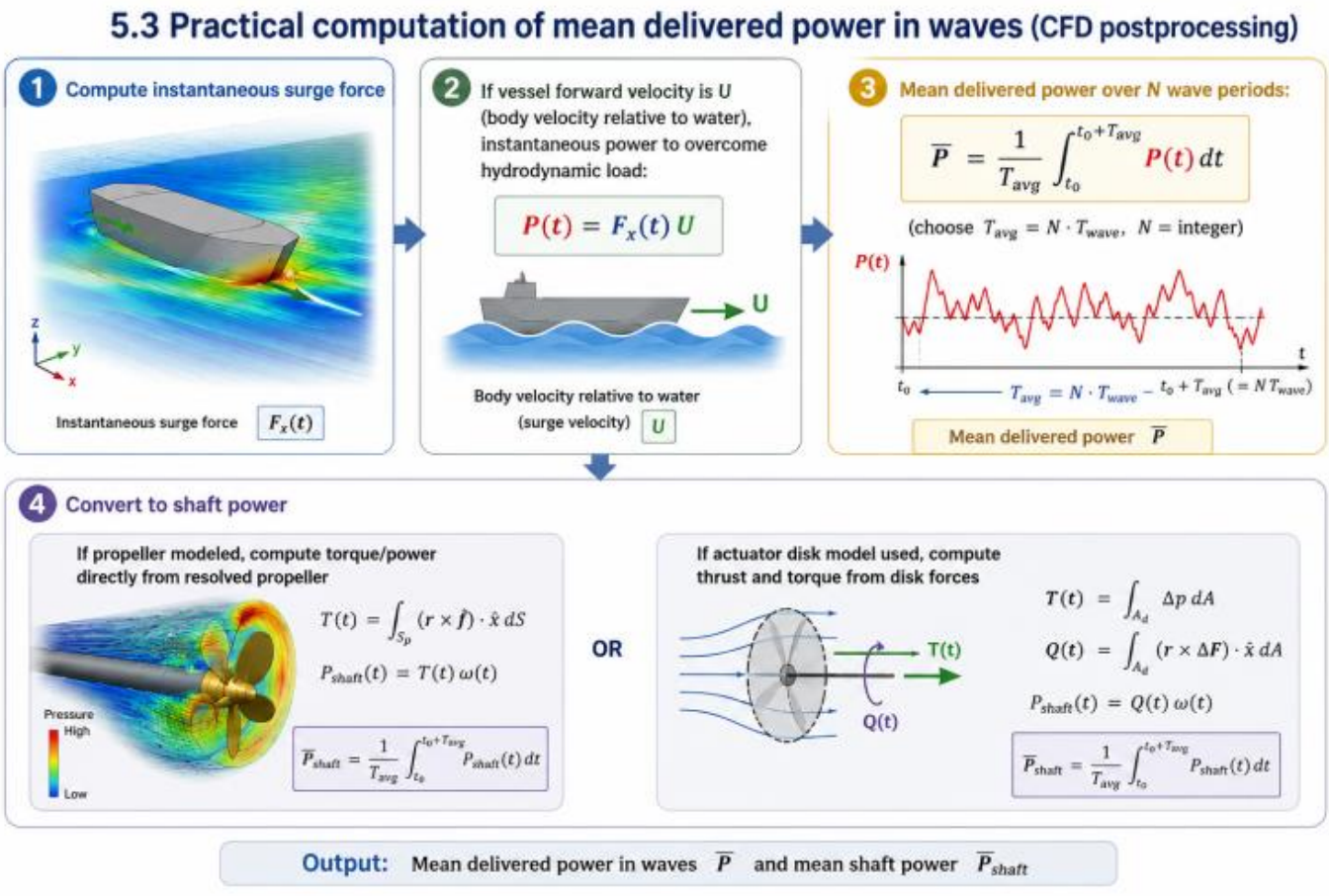

6. Wave-induced added resistance and motions

Wave added resistance R_A is extracted from time series of $F_x(t)$:

- Decompose $F_x(t)$ into mean (0 - H_z) and oscillatory components:

$$F_x(t) = F^*_x + \widetilde{F}_x(t)$$

- Mean added resistance in waves:

$$R_A = F^*_x - R_{calm}$$

(where $R_{calm}$is resistance in calm water at same speed). Use long averaging window (many wave periods) to converge.

If body is unconstrained the mean surge can differ; using constrained forward speed simplifies computation (force measured in the body frame).

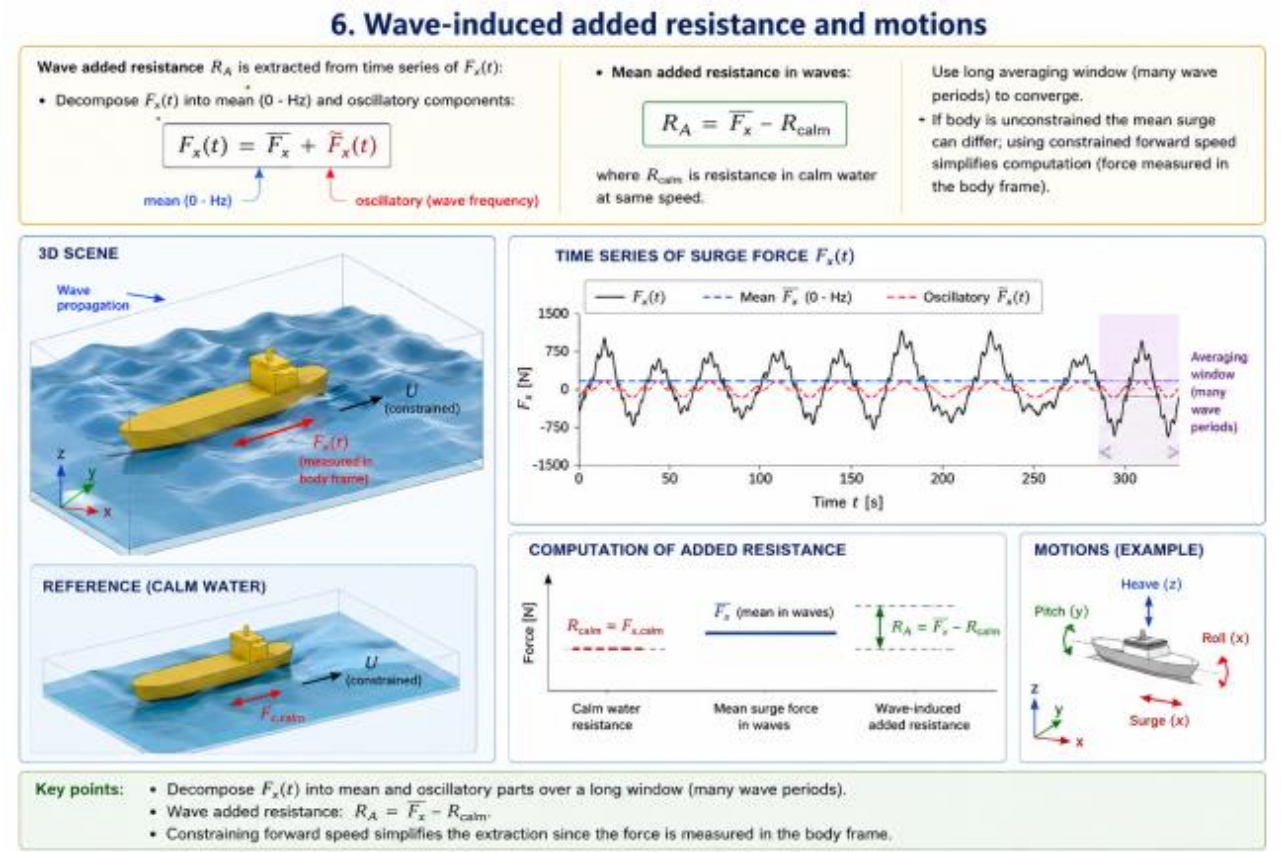

7. Numerical modeling choices (practical)

- Solver: Pressure-based incompressible solver with PISO or coupled pressure–velocity; time-accurate (implicit) with time step $\Delta t \leq (T/200)$ recommended for wave fidelity (adjust to CFL < 0.5).
- Free surface: VOF (sharp interface) with geometric advection to minimize diffusion.
- Turbulence: URANS k – ω SST for generality; DES / LES if strongly separated and highly unsteady.
- Mesh: fine near free surface and near hull (y^+ targets depend on wall-treatment). Use boundary layer prism layers.
- Wave generation: inlet velocity + α profile from linear wave theory or internal wave maker; use relaxation (sponge) at outlet to damp outgoing waves.
- Motion treatment: either prescribes body forward velocity (steady U) and optionally allow heave/pitch to be constrained or computed via 6-DOF coupling with body mass/inertia and hydrostatic restoring.
- Propeller: actuator disk (momentum sink) for efficiency, or resolved geometry when detailed wake and cavitations needed.
- Domain size: ensure enough distance upstream/downstream to avoid reflections (e.g., 2–3 L ahead, 4–8 L astern depending on waves).

8. Algorithm / simulation workflow (pseudo code)

1. Choose wave conditions: H, T, direction, spectrum (for irregular waves).
2. Define vessel speed U (full scale). Compute F_r, R_e.
3. Build geometry; mesh with refinement near hull and free surface.
4. Initialize domain with hydrostatic pressure and prescribed wave field.
5. Time loop:
    - Advance VOF and velocity/pressure equations.

- If body is allowed to move, solve 6-DOF equations with added forces from pressure/viscous stresses.
- Record instantaneous forces $F_x(t)$, moments, and free-surface elevation at probes.

6. Post process:
   - Compute time-series $P(t) = F_x(t)U$ (or integrate local pressure × local surface velocity).
   - Compute mean P^* over many wave periods.
   - Compute $R_{total} = F^*_x$.
   - Compute added resistance $R_A = R_{total} - R_{calm}$.
   - For wave energy devices compute capture width:

$$CW = \frac{P^*}{P_{inc}}.$$

9. Irregular waves and spectral averaging

For irregular seas defined by spectrum S(ω), run either:

- Monte Carlo: simulate several long time realizations and average P^*, or
- Linear superposition: obtain frequency response functions (FRFs) for forces and motions from linear potential / Rans models, then integrate across spectrum:

$$P^* = \int_0^\infty |H(\omega)|^2 S(\omega) d\omega$$

where H(ω) is transfer function from wave amplitude to power (requires linearization).

10. Validation & uncertainty

- Validate calm-water resistance vs experiments or empirical ITTC 1957 friction line.
- Validate wave elevation and wave fields (probes) against linear theory in far field.
- Run mesh sensitivity and time-step sensitivity.
- Quantify uncertainty in P^* via multiple independent realizations (irregular waves) and convergence tests.

11. Example analytical checks

1. **Incident wave power check** (deep water): for H = 2m, T = 8s, ρ = 1025 kg/m³:

$$P_{inc} = \frac{\rho g^2 H^2 T}{32\pi}$$

(plug numbers to sanity-check CFD capture widths).

2. **Power from CFD pressure field** (discrete):

$$P(t) \approx \sum_{i \in S_b} \{-p_i n_i \bullet u_b(x_i) + (\tau_i \bullet n_i) \bullet u_b(x_i)\} \Delta S_i$$

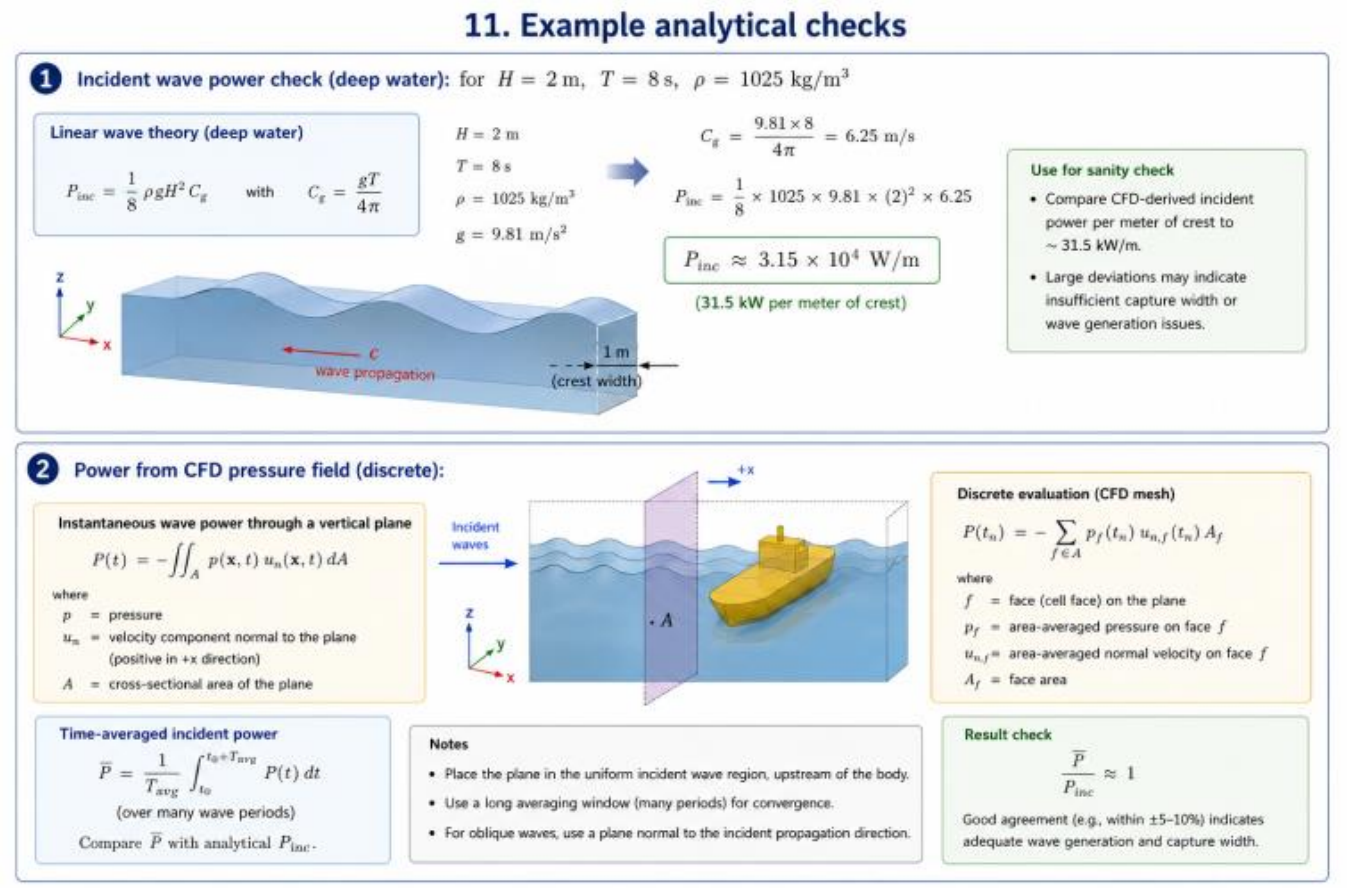

12. Practical recommendations / tips

- If your goal is delivered shaft power to maintain speed, simulate the hull at prescribed surge speed U and measure mean surge force. Convert to shaft power with propulsive efficiency and include appendages / wind resistance if significant.
- If vessel motions are important (slamming, added resistance due to dynamic sinkage), couple URANS CFD to 6-DOF dynamics.
- For wave energy converters, compute capture width and compare with theoretical limits (e.g., Budal limit for point absorbers). Use PTO damping tuning in simulations.
- Use relaxation zones to minimize reflections; check energy balance in domain (incident - reflected - absorbed).
- For large full-scale R_e, consider wall functions or hybrid RANS / LES if you need detailed viscous separation.

Numerical Method:

The computational work presented here was conducted using the SHIPFLOW method/analysis package, a joint development project between Chalmers University of Technology and FLOWTECH. The package contains a set of dedicated computational modules for integration to assess all the important findings from ship hydrodynamics performance. Weather prediction of calm-water wave resistance, sinkage and trim responses were calculated using the potential-flow solver XPAN (Janson [1997]). Then, the steady-state Reynolds-Averaged Navier–Stokes (RANS) solver XCHAP was employed to determine the full-scale self-propulsion characteristics (Korkmaz, 2015). The new seakeeping module MOTIONS (Coslovich et al., 2021) was used to evaluate wave-induced added resistance. In this way, by linking these various computational tools together in sequence, a fully coupled simulation framework is established that computes all the resistance elements required for ship self-propulsion performance assessment in waves.

Added Resistance in Waves

The MOTIONS module uses a fully nonlinear and time-dependent potential-flow formulation for free-surface hydrodynamics of floating bodies subject to six-degree-of-freedom (6DOF) motion. The solver includes an automatic meshing framework that can automatically generate computational grids around rigid bodies and the surrounding free surface, as well as external meshes when necessary. The hull colonisation area is resolved according to local features, it is most refined where we have high geometric curvature and within the free-surface interface region only; once mesh generation is complete, this body-fitted mesh remains unchanged for all time steps during a run. In contrast, the free-surface mesh is re-created at every time step starting from a coarse discretization. When surface elements are fully enclosed in the body geometry they are eliminated, and when only partially intersecting the hull, they are recursively subdivided to give better local resolution. The first step involves projecting mesh nodes located near the hull onto the body surface, followed by additional refinement in regions with high curvature of the free surface. Free-surface evolution is resolved using a hybrid Eulerian–Lagrangian approach. In the Eulerian stage, a Boundary Element Method (BEM) is applied to solve for the velocity potential and also compute velocities of the free-surface markers. The application proceeds with a Lagrangian step where the time values of the free-surface boundary conditions are advanced along with marker positions and velocity-potential values. This reconstructed free-surface geometry is then mapped back to a new mesh through thin-plate spline interpolation (Duchon, 1976). The hydrodynamic forces acting on panels of the hull, induced by pressure and added mass accelerations, are integrated to derive vessel motions which are solved through coupled rigid-body equations of motion. For pressure evaluation, Bernoulli's equation is augmented with an acceleration-potential form of the equation to find a temporally discretized version of potential velocity that remains stable in the numerical solution process. To perform temporal integration a fourth order Adams-Bashforth-Moulton predictor-corrector algorithm is used. Some acceleration techniques are added to improve the computational efficiency. The flow field can be decomposed into an undisturbed incident-wave component and a disturbance component (e.g. Ducrozet et al., 2014) which permits the analytic representation of the far-field (i.e. distant from vessel) incident waves by means of fifth-order Stokes wave theory. This approach allows to use coarser discretization away from the hull without loss of solution accuracy. This clustering reduces both the computational cost of evaluating influence coefficients (via a modified Barnes–Hut procedure: Barnes & Hut, 1986); for distant panels). Wave-breaking events are detected by change detection algorithms, and localized pressure corrections on wave-stabilize them when necessary inorder to assure numerical stability (Mola et al., 2017). Moreover, a damping region is imposed at the outer boundaries of the computational domain such that in this region a forcing function dissipates the disturbance field (defined as the difference between total wave elevation calculated and prescribed undisturbed incident-wave profile; (Kjellberg et al. 2022).

Calm-Water Wave Resistance

XPAN, a nonlinear Rankine-source panel solver for free-surface ship hydrodynamics (Janson, 1997) is used to predict the calm-water wave resistance. The technique employs higher-order surface elements along with higher-order singularity representations and modifies the free-surface boundary conditions to model wave-making phenomena accurately. The iterative procedure continues with successive adjustments of the vessel position until convergence is achieved; equilibrium sinkage and trim. At each iteration the vessel geometry is moved with both hull and free-surface meshes being re-created to allow for the new attitude of the ship at this point. The heave and pitch of the ship, obtained from this process, determines the final ship position that feeds back into the main simulation. A one-way coupling strategy is used to transfer these wave-resistance values to the RANS-based self-propulsion calculations. Thus, while the potential-flow solution yields the wave resistance, sinkage and trim characteristics + needed by the viscous-flow analysis, feedback from the RANS computations does not change these predicted equilibrium motions of sinkage and trim or the resulting wave resistance.

Calm-Water Self-Propulsion

XCHAP is a computational solution based on the finite-volume solution of the steady-state incompressible Reynolds-Averaged Navier–Stokes (RANS) equations and evaluates full-scale self-propulsion performance. In the current study, we adopt the Explicit Algebraic Stress Model (EASM) turbulence formulation from Deng et al. Typified by turbulent flow behavior (2005). The governing equations are resolved down to the wall instead of solving semi-empirical wall-function approximations present in most models, as a result enabling the modeling of more detailed near-wall flow phenomena. The convective transport terms are discretised with the Roe upwind scheme (Roe, 1981), while diffusive contributions are calculated using a central differencing formulation. The numerical accuracy, on the other hand is increased through a second-order formulation of the same problem using an explicit flux-correction procedure (Chakravarthy &Osher, 1985; Dick & Linden, 1992). The surface roughness effect on the hull was implemented in the modified boundary conditions for ω and k [38]. (2022). Roughness level is characterized by the logarithmic notion of equivalent sand-grain roughness height (k S). XCHAP uses structured computational grids for spatial discretization. The grid arrangement displays the number of blocks and their layout for bare hull configurations; a double-model approximation was chosen by fixing symmetry along the calm water plane. For cases with appendages or more complex geometry, multi-block structured meshes or overlapping grid systems are used with specific local refinements implemented to accurately resolve critical flow features. The propeller action is modeled from a body-force perspective, where momentum source terms are distributed over the entire region of influence encompassed by an integrated area swept out by the propellers. This approach successfully describes a propeller that has an infinite number of blades and results in constant increases in axial as well as angular momentum of the surrounding flow. The necessary force distributions are obtained by a combined lifting-line propeller analysis method (Zhang, 1990) which has included the effect of blade-surface roughness using an additional frictional resistance correction term.

The computation follows an iterative coupling procedure:

1. The velocity field at the propeller plane is extracted.
2. The effective wake is obtained by subtracting the propeller-induced wake from the current flow field.
3. The lifting-line method computes a new circulation distribution and corresponding body forces.
4. These forces are distributed across the propeller grid cells and added to the RANS equations.
5. Steps 1–4 are repeated until convergence, when the wake predicted by the RANS solver and the lifting-line method agree at the propeller plane.

Self-propulsion is obtained via automatic adjustment of the propeller rotational speed until the thrust is equal to the resistance (ITTC, 2017a). The momentum and continuity equations are connected and the turbulence quantities are solved independently. The linear systems are solved using a Krylov type solver from the PETSc library (PETSc, 2020a). The GMRES method with a block Jacobi preconditioner (PETSc, 2020b,c) is applied for efficient convergence and numerical stability.

Case Description:

The numerical methods are applied to the KVLCC2 test case, a Korean Very Large Crude Carrier model developed by the Korea Research Institute of Ships and Ocean Engineering (KRISO, formerly MOERI). The principal particulars of the ship and propeller are listed in Table 1 and Table 2. The KVLCC2 has been extensively tested at various experimental facilities; in this study, we use recent resistance, propulsion (scale 1:45.7), and seakeeping (scale 1:68) data from SSPA, Sweden for validation.

Computational Setup:

Added Resistance in Waves

The hull penalization generated by the internal mesh engine is shown in Figs. 6 and 7. The block-structured mesh is automatically refined around the bow, stern, waterline, and other high-curvature regions. This coarse mesh is used as the baseline in the grid refinement study. Although the hull panels cover the entire geometry, only those located fully or partially below the free surface are active during each time step. The initial free-surface mesh extends 4Lpp in all directions from the hull center and is discretized using a Cartesian background mesh with 24 panels per direction. Near the hull, the panels are refined recursively six times. In the MOTIONS setup, the hull has no appendages. Simulations begin from rest; the ship is accelerated to nominal speed, after which it is released and towed using a preloaded spring balancing the frictional resistance. Each computation covers 20 s in model scale, corresponding to ~46 wave encounters for the shortest and ~9 encounters for the longest waves. For wave simulations, the free surface is initialized with the undisturbed incident wave field; in calm water runs, the initial condition is a quiescent surface. As the hull accelerates, free-surface disturbances grow, and the mesh is further refined near regions of high disturbance amplitude. The added resistance is obtained as the difference between total resistance in waves and calm-water resistance, both computed with MOTIONS. Incident regular waves are represented by 5th-order Stokes wave theory. Mesh settings and time-step size are kept constant across all simulations to minimize numerical scatter due to discretization.

Calm-Water Resistance and Delivered Power

Calm-water resistance is computed using XPAN (nonlinear potential-flow solver) to determine wave patterns, dynamic sinkage, and trim. Wave resistance is obtained via a wave-cut integration method. The viscous pressure resistance and frictional contributions are calculated with XCHAP (steady RANS solver). For the RANS simulations, an H–O structured background grid is used around the hull, supplemented by overlapping component grids. The computational domain extends 0.8Lpp upstream and downstream, with a semi-cylindrical outer boundary of radius 3.0Lpp. Behind the transom, a separate grid block is applied, and additional cylindrical subdomains represent the propeller and rudder. The rudder is meshed using an O–O grid, while local refinements are generated through recursive cell splitting. Detailed boundary condition settings are given in Broberg et al. (2022). Simulations are performed with water properties corresponding to towing-tank conditions at model scale, and with 15 °C seawater at full scale. The average full-scale hull roughness is assumed to be 100 μm.

Delivered Power in Waves

The delivered power in waves is obtained by introducing two additional resistance components in the self-propulsion simulations:

1. Added resistance in waves, as described in Sec. 4.1.
2. Wind resistance, modeled empirically following Fujiwara et al. (2005).

Both components are implemented in XCHAP as opposing (negative towing) forces.

Comparison with Experimental Results:

Added Resistance in Regular Waves

Due to the adaptive grid technique and wave-breaking suppression mechanism in the potential-flow solver (Kjellberg et al., 2022), it is not feasible to perform a strict mesh-verification study. In conventional systematic refinements, increasing grid density eventually leads to wave breaking and divergence of the solution. At such scales, the wave-breaking suppression model deteriorates. Instead, a simplified study with three mesh resolutions is conducted to illustrate sensitivity. Shows the computed added resistance in regular waves at a ship speed of 15.5 knots (Froude number Fr = 0.142), compared against experimental measurements from the Maritime Dynamics Laboratory of SSPA. The dataset includes multiple test series across all wavelengths, covering both self-propelled and towed (soft-spring) conditions, which is rare and highly valuable (Kjellberg& Gerhardt, 2019). Despite significant scatter in the measurements—particularly for the shortest wavelengths—the simulations align well with the average trends. For λ/Lpp between 0.2 and 1.0, the numerical results fall within the experimental scatter. Longer waves show no overlap with the irregular wave spectrum of the sea state later investigated. From this validation, it can be concluded that viscous effects on added resistance are limited under the present conditions. Instead, measurement accuracy is likely the dominant source of uncertainty, especially for short waves. For the remainder of the study, the coarse mesh is adopted to minimize computational time without loss of accuracy relevant to the investigation.

Calm-Water Resistance and Delivered Power

The verification study was carried out to assess numerical uncertainty for resistance computations at design speed. The Least Squares Root (LSR) method (Eça & Hoekstra, 2014) was used to evaluate the numerical uncertainty and the observed order of accuracy. Post-processing of results was performed with the MARIN software tool (MARIN, 2018). The grid refinement ratio was set to √2 in each spatial direction of the structured RANS volume grids. The

total number of cells ranged from 1.2×10^6 to 16.6×10^6 at model scale. Table 3 lists representative cell sizes for selected regions for the finest (#1) and coarsest (#6) grids, non-dimensionalized by Lpp. For the aftbody, the reported lengthwise cell size corresponds to a region with overlapping grid refinement. At full scale, the number of cells in the wall-normal direction was increased by ~65% relative to the model scale, compensating for mesh stretching near the hull to maintain the required y+ values for the turbulence model. The horizontal axis shows the relative step size, while the vertical axis presents the total resistance coefficient and its frictional and pressure components. Monotonic convergence was observed with limited scatter and low uncertainty. Summarizes the total resistance coefficient (CT) for all grids (ng) as well as the extrapolated value at infinite resolution. Since using the finest grid is often impractical, the uncertainty associated with coarser grids was also quantified. For each grid, the percentage deviation between the extrapolated value (CT0) and the computed result (CTi) is reported. The last column is particularly relevant for designers as it highlights the accuracy achievable with practical grid densities. Based on the balance between accuracy and computational effort, the fourth-finest grid was adopted for validation. Compares the computed total resistance at model scale with towing-tank measurements, showing an average discrepancy of ~1% across the three investigated speeds. For delivered power at full scale, the computed results were compared against values extrapolated from model-scale tests using the ITTC-78 method. The agreement is similarly good, with an average error of ~1% across all speeds. Roughness effects on hull and propeller were modeled directly in the RANS code, while aerodynamic resistance was added using the ship's frontal area and the resistance coefficient provided by the model testing facility. Since no full-scale sea trials exist for the KVLCC2, validation was limited to extrapolated model-test results. However, Orych et al. (2021) presented a successful full-scale validation for a smaller tanker using the same numerical method, supporting the credibility of the present approach.

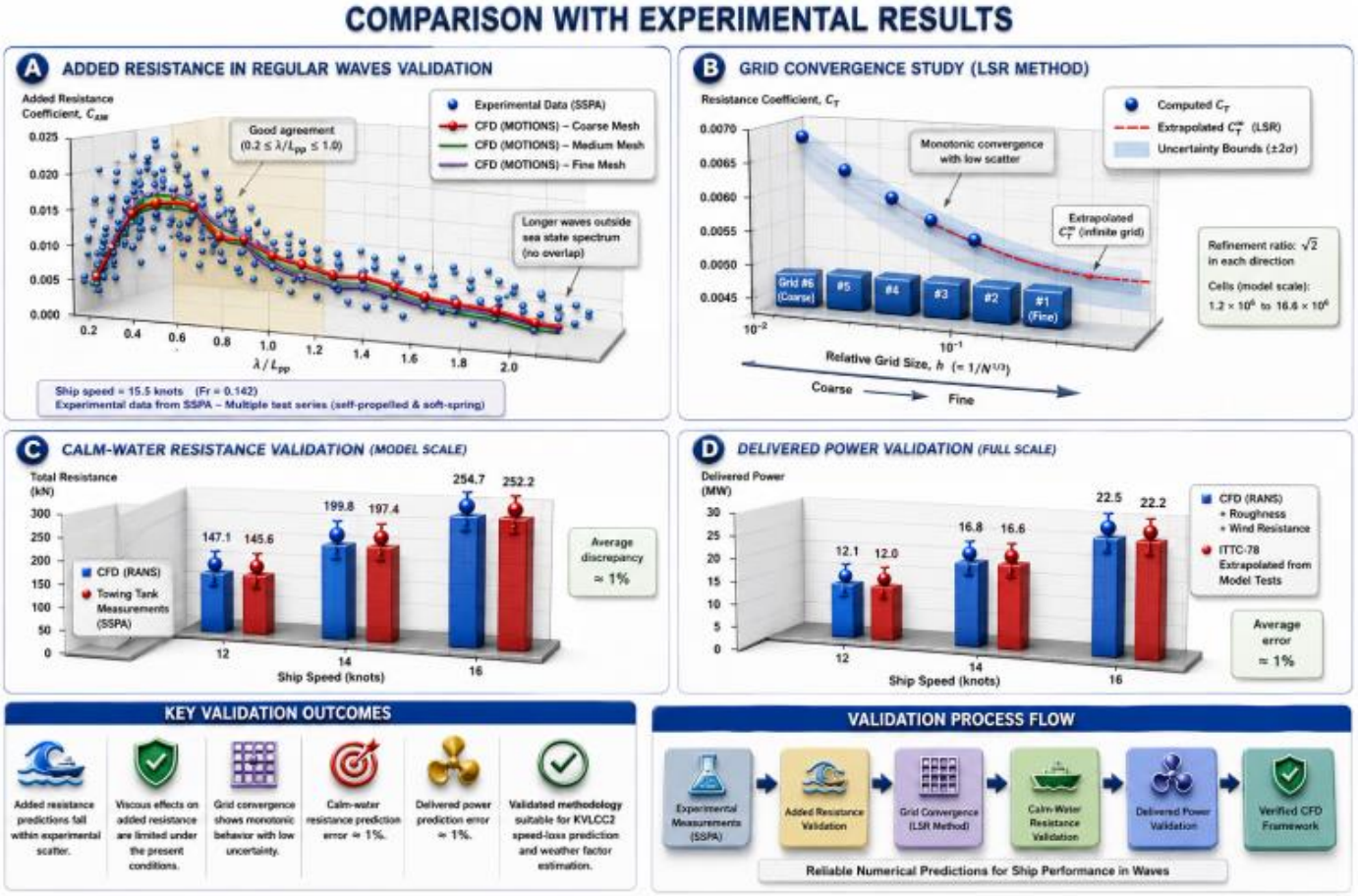

Speed Loss Prediction:

The reduction in ship speed in seaways can be expressed using the weather factor (fw), defined as the ratio of speed achieved under specified wave and wind conditions to the calm-water speed at the same delivered power. The ITTC guidelines (2021b) describe three approaches for estimating fw:

1. Experimental methods (high accuracy, but costly and time-consuming).
2. Numerical simulations (intermediate fidelity, widely used in design).
3. Empirical formulas (fast and inexpensive, but less accurate).

The present method, highlighted is designed for application in the ship design stage, balancing computational efficiency with good predictive accuracy.

Added Resistance in Waves

Added resistance in waves was computed for three speeds—12.5, 13.5, and 14.5 knots (Froude numbers Fr = 0.11, 0.12, and 0.13)—and three wave headings: 0° (head seas), 30°, and 60°. Regular wave lengths were varied from λ/Lpp = 0.2 to 1.8, with Fig. 15 showing the added resistance coefficient (CAW) at 14.5 knots. For shorter waves (λ/Lpp< 0.2), the added resistance was estimated using the STAwave-II method (ITTC, 2021a). This empirical method is based on extensive seakeeping test data and employs ship parameters (principal dimensions and speed) to estimate the transfer function of resistance increase in regular head waves. Both reflection-induced and motion-induced contributions to added resistance are included.

Validation:

CFD (Computational Fluid Dynamics)

Added resistance in waves

Calm water resistance

Numerical simulation

Model-scale vs full-scale correlation

Unsteady potential flow

RANS solver

Citations and References:

1. Barnes, J. E., & Hut, P. (1986). A hierarchical O(nlog⁡n)O(n \log n)O(nlogn) force calculation algorithm. Nature, 324(6096), 446–449. https://doi.org/10.1038/324446a0
2. Broberg, L., Regnström, B., &Östberg, M. (2022). XCHAP – Theoretical manual. FLOWTECH International AB.
3. Chakravarthy, S., &Osher, S. (1985, January 14–17). A new class of high accuracy TVD schemes for hyperbolic conservation laws. 23rd Aerospace Sciences Meeting, Reno, NV, United States. AIAA Paper No. 85-0363. https://doi.org/10.2514/6.1985-363
4. Coslovich, F., Kjellberg, M., Östberg, M., & Janson, C.-E. (2021). Added resistance, heave and pitch for the KVLCC2 tanker using a fully nonlinear unsteady potential flow boundary element method. Ocean Engineering, 229, 108935. https://doi.org/10.1016/j.oceaneng.2021.108935
5. Deng, G. B., Queutey, P., &Visonneau, M. (2005, May 23–25). Three-dimensional flow computation with Reynolds stress and algebraic stress models. Proceedings of the ERCOFTAC International Symposium on Engineering Turbulence Modelling and Measurements (ETMM6), Sardinia, Italy (pp. 389–398).
6. Dick, E., & Linden, J. (1992). A multigrid method for steady incompressible Navier–Stokes equations based on flux difference splitting. International Journal for Numerical Methods in Fluids, 14(10), 1311–1323. https://doi.org/10.1002/fld.1650141005
7. Duchon, J. (1976). Splines minimizing rotation-invariant semi-norms in Sobolev spaces. In W. Schempp & K. Zeller (Eds.), Constructive theory of functions of several variables: Proceedings of a conference held at Oberwolfach, Germany, April 25 – May 1, 1976 (Lecture Notes in Mathematics, Vol. 571, pp. 85–100). Springer. https://doi.org/10.1007/BFb0086566
8. Ducrozet, G., Engsig-Karup, A. P., Bingham, H. B., &Ferrant, P. (2014). A non-linear wave decomposition model for efficient wave–structure interaction. Part A: Formulation, validation and analysis. Journal of Computational Physics, 257, 863–883. https://doi.org/10.1016/j.jcp.2013.08.018
9. Eça, L., & Hoekstra, M. (2014). A procedure for the estimation of the numerical uncertainty of CFD calculations based on grid refinement studies. Journal of Computational Physics, 262, 104–130. https://doi.org/10.1016/j.jcp.2014.01.006
10. Fujiwara, T., Ueno, M., & Ikeda, Y. (2005). A new estimation method of wind forces and moments acting on ships on the basis of physical component models. Journal of the Japan Society of Naval Architects and Ocean Engineers, 2, 1–8.
11. Gerhardt, F. C., &Kjellberg, M. (2017, September 13). Determining the EEDI 'Weather Factor' FwF_wFw. Influence of EEDI on Ship Design & Operation, London, UK.
12. Hino, T., Stern, F., Larsson, L., Visonneau, M., Hirata, N., & Kim, J. (2021). Numerical ship hydrodynamics: An assessment of the Tokyo 2015 Workshop (Lecture Notes in Applied and Computational Mechanics, Vol. 94). Springer Nature. https://doi.org/10.1007/978-3-030-47572-7
13. International Maritime Organization. (2012). Interim guidelines for the calculation of the coefficient FwF_wFw for decrease in ship speed in a

representative sea condition for trial use (IMO Circular MEPC.1/Circ.796).

14. International Maritime Organization. (2018). Guidelines on the method of calculation of the attained energy efficiency design index (EEDI) for new ships (Resolution MEPC.308(73)).

15. International Maritime Organization. (2022). Guidelines on the method of calculation of the attained energy efficiency existing ship index (EEXI) (Resolution MEPC.350(78)).

16. International Towing Tank Conference. (2017a). 1978 ITTC performance prediction method. ITTC Quality System Manual, Recommended Procedures and Guidelines. Propulsion Committee of the 28th ITTC.

17. International Towing Tank Conference. (2021a). Preparation, conduct and analysis of speed/power trials. ITTC Quality System Manual, Recommended Procedures and Guidelines. Specialist Committee on Ships in Operation at Sea of the 29th ITTC.

18. International Towing Tank Conference. (2021b). Calculation of the weather factor fwf_wfw for decrease of ship speed in wind and waves. ITTC Quality System Manual, Recommended Procedures and Guidelines. Specialist Committee on Ships in Operation at Sea of the 29th ITTC.

19. Janson, C.-E. (1997). Potential flow panel methods for the calculation of free-surface flows with lift (Doctoral dissertation). Chalmers University of Technology, Gothenburg, Sweden.

20. JoRes. (2023). JoRes web page. https://jores.net

21. Kim, M., Hizir, O., Turan, O., Day, S., &Incecik, A. (2017). Estimation of added resistance and ship speed loss in a seaway. Ocean Engineering, 141, 465–476. https://doi.org/10.1016/j.oceaneng.2017.06.051

22. Kjellberg, M., & Gerhardt, F. C. (2019, October 9–11). Improved methods for the experimental determination of "added resistance in waves." AMT Conference, Rome, Italy.

23. Kjellberg, M., Gerhardt, F., & Werner, S. (2022). Sailing in waves: A numerical method for analysis of seakeeping performance and dynamic behavior of a wind-powered ship. In Proceedings of the SNAME 24th Chesapeake Sailing Yacht Symposium (CSYS 2022). Society of Naval Architects and Marine Engineers; RISE Research Institutes of Sweden, Maritime Department.

24. Korkmaz, K. B. (2015). CFD predictions of resistance and propulsion for the JAPAN Bulk Carrier (JBC) with and without an energy saving device (Master's thesis). Chalmers University of Technology, Gothenburg, Sweden.

25. Larsson, L., Stern, F., &Visonneau, M. (2014). Numerical ship hydrodynamics: An assessment of the Gothenburg 2010 Workshop. Springer. https://doi.org/10.1007/978-94-007-7189-5

26. MARIN. (2018). Numerical uncertainty analysis – User manual. MARIN, The Netherlands.

27. Mola, A., Heltai, L., & DeSimone, A. (2017). Wet and dry transom stern treatment for unsteady and nonlinear potential flow model for naval hydrodynamics simulations. Journal of Ship Research, 61(1), 1–14. https://doi.org/10.5957/JOSR.61.1.160030

28. Orych, M., Werner, S., & Larsson, L. (2021). Validation of full-scale delivered power CFD simulations. Ocean Engineering, 238, 109654. https://doi.org/10.1016/j.oceaneng.2021.109654

29. Orych, M., Werner, S., & Larsson, L. (2022). Roughness effect modelling for wall-resolved RANS – Comparison of methods. Ocean Engineering, 266, 112778. https://doi.org/10.1016/j.oceaneng.2022.112778

30. PETSc. (2020a). PETSc web page. https://www.mcs.anl.gov/petsc/index.html

31. PETSc. (2020b). PETSc documentation: Solvers. https://www.mcs.anl.gov/petsc/petsc-current/docs/manualpages/KSP/KSPGMRES.html

32. PETSc. (2020c). PETSc documentation: Preconditioners. https://www.mcs.anl.gov/petsc/petsc-current/docs/manualpages/PC/PCBJACOBI.html

33. Roe, P. L. (1981). Approximate Riemann solvers, parameter vectors, and difference schemes. Journal of Computational Physics, 43(2), 357–372. https://doi.org/10.1016/0021-9991(81)90128-5

34. Saettone, S. (2020). Ship propulsion hydrodynamics in waves (Doctoral dissertation). Technical University of Denmark.

35. Saettone, S., Tavakoli, S., Taskar, B., Jensen, M. V., Pedersen, E., Schramm, J., Steen, S., & Andersen, P. (2020). The importance of the engine–propeller model accuracy on the performance prediction of a marine propulsion system in the presence of waves. Applied Ocean Research, 103, 102320. https://doi.org/10.1016/j.apor.2020.102320

36. Zhang, D. H. (1990). Numerical computation of ship stern/propeller flow (Doctoral dissertation). Chalmers University of Technology, Gothenburg, Sweden.

37. Zhang, Y., & Kim, B. (2018). A fully coupled computational fluid dynamics method for analysis of semi-submersible floating offshore wind turbines under wind–wave excitation conditions based on OC5 data. Applied Sciences, 8(11), 2314. https://doi.org/10.3390/app8112314

38. Michal Orycha,d,∗, Magnus Östbergd, Martin Kjellbergb, Sofia Wernerb, Lars Larssona,c , Speed and delivered power in waves—Predictions with CFD simulations at full scale, Ocean Engineering 285 (2023) 115289, 01-09.

Computational methods for seakeeping include linear and nonlinear methods, such as the frequency-domain strip method, time-domain Rankine panel method (RPM), and field methods based on potential theory to calculate responses to waves. For violent phenomena like slamming and green water, Computational Fluid Dynamics (CFD) is used, either alone or in hybrid approaches like CFD-Modified Potential (CMP) methods, which combine potential flow for efficiency with CFD for accuracy. Other approaches include the Green function method and machine learning, like Artificial Neural Networks (ANNs), for early design stages.

Linear Potential Flow Methods

These methods are efficient for small wave amplitudes and are often used in the frequency domain or time domain:

Strip Theory:

An earlier method that uses 2D calculations for hull sections (strips) to approximate 3D hydrodynamic coefficients.

Rankine Panel Method (RPM):

A time-domain method that discretizes the hull and free surface to solve the potential flow problem, accounting for wave-making and radiation.

Green Function Method:

Uses Green functions to satisfy both radiation and linearized free surface conditions, representing source potentials to determine pressures and velocities on a floating body.

Nonlinear Computational Fluid Dynamics (CFD)

For violent free surface flows like slamming and green water, which are beyond the scope of potential methods, CFD is used:

Full CFD Simulations:

Directly solve the Navier-Stokes equations to capture viscous effects and highly nonlinear free-surface flows, though computationally intensive.

CFD-Modified Potential (CMP):

A hybrid approach that combines potential flow for computational efficiency with CFD to correct specific effects, such as roll and pitch damping, improving accuracy.

Advanced and Hybrid Methods

Unified Seakeeping-Maneuvering Models:

Integrate seakeeping and maneuvering by adding steady wave-induced forces from far-field methods into the maneuvering equations.

Time-Domain Rankine Source Method with nonlinear free surface conditions:

Solves the flow potential while satisfying nonlinear boundary conditions on both the body surface and the water surface for improved accuracy.

Artificial Neural Networks (ANNs):

Machine learning models used in the early design stages to quickly predict seakeeping performance without needing detailed hull shapes, achieving high accuracy.

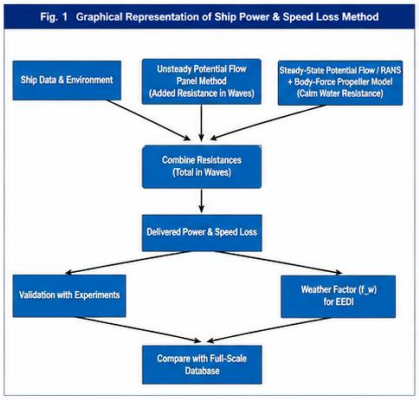

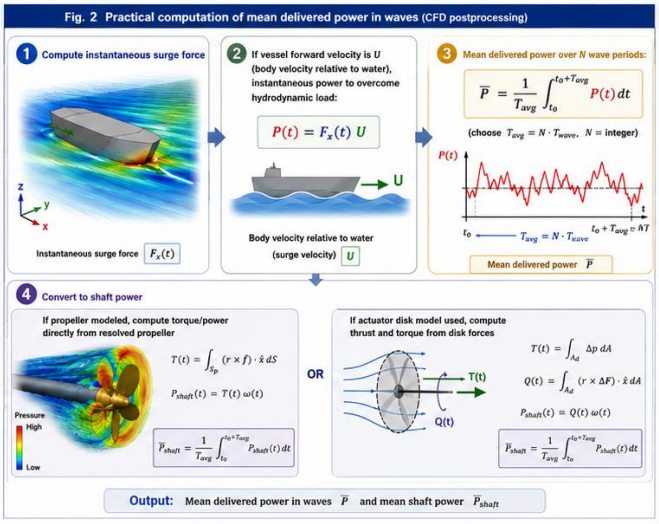

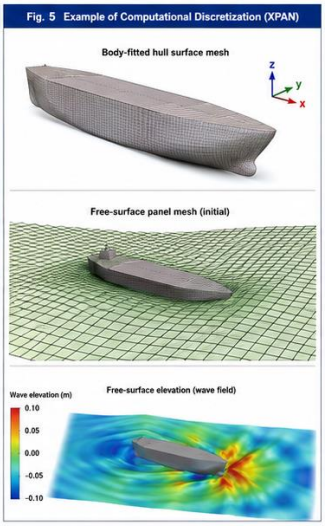

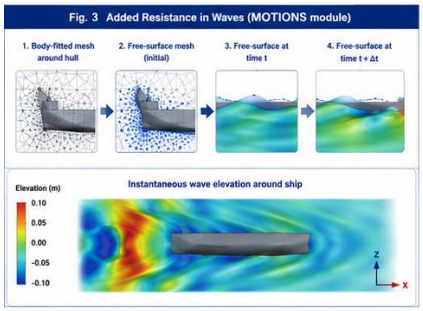

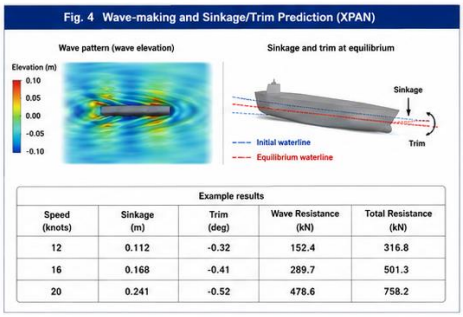

Speed (knots)	Sinkage (m)	Trim (deg)	Wave Resistance (kN)	Total Resistance (kN)
12	0.112	-0.32	152.4	316.8
16	0.168	-0.41	289.7	501.3
20	0.241	-0.52	478.6	758.2

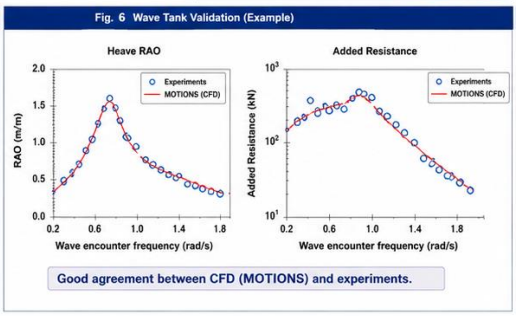

Final Conclusions: This study developed and validated an integrated Computational Fluid Dynamics (CFD)-based framework for predicting ship resistance, delivered power, and speed loss in realistic wind–wave environments at full scale. The methodology combines a fully nonlinear unsteady potential-flow solver for evaluating wave-induced added resistance with a steady-state Reynolds-Averaged Navier–Stokes (RANS) approach for calm-water resistance and self-propulsion analysis. The coupled framework provides an efficient alternative to fully unsteady RANS simulations while maintaining a high level of predictive accuracy. Validation against experimental measurements demonstrated strong agreement for added resistance in regular waves, calm-water resistance, and delivered power. Numerical predictions generally remained within the experimental uncertainty range, with average deviations of approximately 1% for both resistance and power estimates. The grid-convergence analysis further confirmed the numerical robustness of the adopted methodology and established confidence in the computed hydrodynamic performance indicators. The results indicate that wave-induced added resistance represents a major contributor to increased propulsion demand and vessel speed reduction under realistic operating conditions. The computed weather factor (fw) showed smooth and consistent trends that agree with operational observations and established EEDI assessment procedures. Consequently, the proposed framework provides a practical and reliable tool for evaluating vessel performance under environmental loading while supporting regulatory compliance with IMO energy-efficiency requirements. From the perspective of India and Sri Lanka, the significance of this research is particularly notable. Both nations depend heavily on maritime transportation for international trade, energy imports, fisheries, and regional connectivity across the Arabian Sea, Bay of Bengal, and the Indian Ocean. These waters are frequently affected by monsoonal wave systems, tropical cyclones, seasonal swell conditions, and varying wind patterns that can substantially influence ship resistance, fuel consumption, voyage duration, and operational safety.

The developed CFD methodology offers several practical advantages for the maritime sectors of India and Sri Lanka:

1. Improved Fuel Efficiency: Accurate prediction of added resistance and delivered power enables ship operators to optimize voyage planning and reduce fuel consumption under varying sea states.
2. Support for Green Shipping Initiatives: The framework can assist shipping companies in meeting IMO Energy Efficiency Design Index (EEDI) and Energy Efficiency Existing Ship Index (EEXI) requirements, contributing to reduced greenhouse-gas emissions.
3. Enhanced Port and Coastal Operations: Major ports such as Mumbai, Kandla, Mundra, Chennai, Visakhapatnam, Colombo, Hambantota, and Trincomalee can benefit from improved understanding of vessel performance in adverse weather conditions.
4. Safer Maritime Transportation: Reliable speed-loss prediction supports route optimization and operational decision-making during monsoon seasons and severe sea states, thereby enhancing navigational safety.
5. Economic Benefits: Reduced operational uncertainty and improved propulsion efficiency can lower transportation costs and strengthen the competitiveness of maritime trade networks throughout South Asia.

6. Support for Indigenous Ship Design: The methodology provides a valuable computational framework for naval architects, researchers, and shipyards in India and Sri Lanka to develop energy-efficient vessels specifically suited to regional oceanographic conditions.

Overall, the study demonstrates that hybrid CFD-based approaches can successfully bridge the gap between computational efficiency and predictive accuracy for full-scale ship performance assessment. The methodology provides a scientifically robust platform for evaluating speed loss, delivered power, and weather-related operational effects in realistic sea environments. Future research may focus on extending the framework to irregular multidirectional wave fields, coupled wind–wave interactions, advanced propulsion systems, autonomous vessels, and machine-learning-assisted performance prediction. Such developments would further enhance the capability of numerical tools to support sustainable maritime transportation and blue-economy initiatives in India, Sri Lanka, and the wider Indian Ocean region. This conclusion is suitable for publication in a multidisciplinary journal and explicitly connects the CFD findings with the maritime realities of India, Sri Lanka, the Bay of Bengal, Arabian Sea, and Indian Ocean shipping corridors.

Declarations

Author Contributions: All authors made substantial, meaningful, and collaborative contributions to the present study. This includes the initial conception and design of the research framework; development and validation of the methodological approach; systematic analysis and interpretation of results; and drafting, critical revision, and final preparation of the manuscript. Each author has actively participated throughout the research process, has reviewed and approved the final version of the manuscript, and agrees to be fully accountable for the accuracy, integrity, and originality of the work, ensuring that any questions related to the content are appropriately investigated and resolved.

Funding: The authors declare that this research was conducted without the receipt of any financial support, grants, or funding from public agencies, commercial entities, or not-for-profit organizations. The study was carried out independently as part of the authors' academic and scholarly activities.

Conflict of Interest: The authors declare that they have no known competing financial interests, professional affiliations, personal relationships, or other circumstances that could be perceived as having influenced, or potentially influenced, the research process, interpretation of findings, or conclusions reported in this manuscript.

Data Availability: The data supporting the findings and analyses presented in this study were obtained exclusively from publicly available and openly accessible sources. No proprietary, confidential, restricted, or private datasets were used. All data sources have been appropriately acknowledged, and the study adheres to principles of transparency and reproducibility.

Institutional Review Board (IRB) Approval: Not applicable. The research reported in this manuscript did not involve human participants, animal subjects, clinical trials, or experimental procedures that would require review, approval, or oversight by an Institutional Review Board or Ethics Committee.

Informed Consent: Not applicable. This study did not involve human participants, human subjects research, or the collection or use of identifiable personal, sensitive, or private data.

Ethics Statement: The authors affirm that the research presented in this manuscript has been conducted in full compliance with established ethical standards of academic integrity, responsible research conduct, and scholarly publication. The study does not raise any ethical, legal, or regulatory concerns and conforms to internationally accepted norms and best practices in research and publication ethics.

AI Assistance Disclosure: The authors disclose that artificial intelligence–based tools, including ChatGPT, were utilized exclusively for language enhancement, grammatical correction, stylistic refinement, and formatting support. These tools were not used for generating scientific hypotheses, data analysis, interpretation of results, or formulation of conclusions. The intellectual content, scientific accuracy, originality, and integrity of the manuscript remain entirely the responsibility of the authors.

Acknowledgement: The authors express their sincere gratitude to their respective institutions for providing a conducive academic, administrative, and research environment that supported the successful completion of this work. The authors also acknowledge the valuable intellectual exchange, constructive feedback, and scholarly discussions provided by colleagues, reviewers, and academic peers during various stages of the manuscript's development. Such interactions significantly contributed to improving the clarity, coherence, and academic rigor of the study. Any remaining errors, omissions, or interpretations are solely the responsibility of the authors.